Pore Size and Volume Effects on the Incorporation of Polymer into Macro- and Mesoporous Zirconium Titanium Oxide Membranes

Glenna L. Drisko,[†] Lu Cao,[†] Maryline Chee Kimling,[†] Simon Harrisson,[‡] Vittorio Luca,*[,§] and Rachel A. Caruso*[,†,||]

Particulate Fluids and Processing Centre, School of Chemistry, The University of Melbourne, Melbourne, Victoria 3010, Australia, Molecular and Health Technologies, Commonwealth Scientific and Industrial Research Organisation, Clayton South, Victoria 3169, Australia, Materials Science and Engineering, Commonwealth Scientific and Industrial Research Organisation, Clayton South, Victoria 3169, Australia, and Institute of Materials Engineering, Australian Nuclear Science and Technology Organization, New Illawara Road, Lucas Heights, New South Wales 2234, Australia

ABSTRACT Macro- and mesoporous hybrid materials have applications in the fields of drug delivery, catalysis, biosensing, and separations. The pore size requirements must be well-understood to maximize the performance (e.g., load capacity and accessibility) of such materials. Hybrid materials were prepared by coating five distinct macroporous commercial membranes with zirconium titanium oxide through sol−gel chemistry. Calcination of these templated materials produced oxide membranes which had a suite of macropore and mesopore architectures, pore volumes, and surface areas. These differences in physical properties were used to conduct a fundamental study on the relationship between the pore size and volume and the polymer incorporation. Metal oxide membranes were postsynthetically modified with poly(ethyleneimine) (PEI) ranging in molecular weight from 1300 to 1 000 000 Da (1.2−11 nm in hydrodynamic diameter). The incorporation of the polymer from a 9 wt % solution at pH 10 was highly dependent on the pore size and pore volume. As the surface area increased, loading capacity decreased, indicating that much of the increased internal surface, due to small pore diameters (≤8 nm), was inaccessible to the macromolecules. Exclusion of PEI from small mesopores was apparent even for the lowest molecular weight polymer. A high maximum loading of 1.25 mg m^{-2} of 600 000−1 000 000 Da PEI was achieved in the metal oxide with the largest minimum mesopore diameter. Thus, mesopore diameter and pore volume must be considered when designing a mesoporous solid support.

KEYWORDS: composite materials • hierarchical pore structures • hybrid materials • titanium dioxide • zirconium dioxide • surface modification • polyethyleneimine • template synthesis

INTRODUCTION

Hybrid (inorganic−organic) materials are found in many familiar products, such as car parts (1), cosmetics (2), and inks (3). They are also being developed for emerging energy technologies (4, 5), biomedical devices (6), selectively permeable barriers (7), and many more applications (8). Inorganic supports are attractive for applications which require the matrix to be hard, durable, of high surface area, chemically stable, and radiation tolerant. The incorporation of organic moieties within such supports provides enhanced functionality: for example, selective metal adsorption (9) or catalytic activity (10). Recent investigations also include the postsynthetic incorporation of macromolecules into porous silica supports for potential drug delivery devices (11−13). Despite how ubiquitous hybrid materials are today, there have been few studies of the relationship between the solid support structure and the incorporation of large molecules.

Postsynthetic modification is the best synthetic route to hybrid materials when the solid support must be calcined at temperatures which would damage the organic component, when the synthetic conditions (e.g., pH) would harm the organic functionality, and when one must avoid burying the organic molecules within the walls of the solid support. In the case of postsynthetic incorporation, the pore size of the support is very important. Small pores produce higher surface areas, potentially allowing more adsorption of macromolecules; however, if the pores are too small, macromolecules will not be able to enter (14, 15). In one example, enzyme loading was highest within a confined pore system (14), but in another, polyelectrolyte loading was greatest for

* To whom correspondence should be addressed. E-mail: rcaruso@unimelb.edu.au (R.A.C.); vluca@cnea.gov.ar (V.L.).

Received for review September 9, 2009 and accepted October 26, 2009

[†] The University of Melbourne.

[‡] Molecular and Health Technologies, Commonwealth Scientific and Industrial Research Organisation.

[§] Australian Nuclear Science and Technology Organization. Current address: CNEA Gerencia Quimica, Av. General Paz 1499, 1650 San Martin, Provincia de Buenos Aires, Argentina.

[||] Materials Science and Engineering, Commonwealth Scientific and Industrial Research Organisation.

DOI: 10.1021/am9006098

the support with the largest mesopores (15). Hence, the morphology of an inorganic support must be precisely controlled and the pore size constraints well-understood. Thus far, all fundamental studies have been performed on porous submicrometer sized particles (14, 15) and thin films, where diffusion has not been of large concern (16−18). It is important to study pore size restraints on macroscopic materials. Additionally, materials containing hierarchical pores can combine the benefits of a rapidly accessible surface in combination with the high surface area of mesostructured materials.

Inorganic membranes are interesting because of their ultrafiltration performance (19). However, organic-functionalized membranes could further enhance their potential in catalysis and separations. For instance, membranes impregnated with large enzymes could be useful in catalytic synthesis and as sensors. Membranes modified with polymers could be used to adsorb metals or other organic molecules. We have previously demonstrated that membrane templates can produce metal oxides with reproducible pore structure (20−23). In this article, the technique has been extended to mixed zirconium titanium oxides and the characterization of these materials. A selection of five commercially available membranes were used to prepare materials with differing properties. The polymer loading capacity was correlated with the variations in the pore architecture (pore size and pore volume) and surface area of the metal oxide supports using 3 molecular weights of poly(ethyleneimine) (PEI).

PEI was chosen as a macromolecular probe because it is available commercially in a variety of molecular weights (1300−1 000 000 Da studied here) and because it can interact electrostatically with the surface of the metal oxide (24). This last point is important to allow a rapid establishment of equilibrium between the bound polymer and nonassociated polymer. Additionally, PEI is an inexpensive, hyperbranched polymer suitable for industrial processes, with an affinity for both organic pollutants (25, 26) and a large range of toxic metals (27−32). There are a limited number of reports on PEI−metal oxide hybrid materials, and most involve PEI surface modification of metal oxide nanoparticles (24, 33−37). None of these reports study the adsorption of PEI within the mesopore surfaces of metal oxides. The preparation of PEI-impregnated titania filters has been reported (26), but the relationship between incorporation and the porosity of the material was not studied. In one report, macroporous alumina membranes with surface areas of 2.2−3.5 $m^2\ g^{-1}$ were modified with PEI and it was found that incorporation was proportional to the surface area (25). The alumina membranes were not mesoporous, so were unlike those in this report, which contain both meso- and macroporosity. PEI-functionalized inorganic membranes could find application in water purification.

EXPERIMENTAL SECTION

Materials and Instrumentation. The sources of the metal oxide precursors were 70% zirconium(IV) propoxide (Sigma Aldrich) and 97% titanium(IV) isopropoxide (Sigma Aldrich), which were diluted with 2-propanol (Univar). Four membranes with a minimum particle retention of 0.2 μm were employed: cellulose acetate (CA), GH Polypro (GHP 0.2 μm), Nylaflo (NY), and Versapor (VERS). A fifth membrane, GH Polypro with a minimum particle retention of 0.45 μm (GHP 0.45 μm), was also used. GHP 0.2 and 0.45 μm, NY, and VERS were purchased from Pall Corp., and CA was obtained from GE Osmonics. The hyperbranched PEI was purchased as such: a 50 wt % solution in water with a molecular weight (M_w) of 1300 Da (Aldrich), neat with M_w = 25 000 Da (Aldrich) and a 50 wt % solution in water with M_w = 600 000−1 000 000 Da (Fluka).

Thermogravimetric analysis (TGA) was carried out using a Mettler Toledo TGA/SDTA 851^e. Mettler STAR^e software was used to analyze the data. To estimate PEI loading in the metal oxide support, samples were heated under oxygen from 20−120 at 10 °C min^{-1}, held at 120 °C for 20 min, then further heated from 120−800 at 10 °C min^{-1}.

Attenuated total reflectance Fourier transform infrared (ATR-FTIR) spectra were recorded by transmittance using a Nicolet Magna 560 instrument, equipped with a liquid nitrogen cooled MCT-A detector. Membranes were ground and pressed into KBr pellets.

The surface area and pore sizes of the synthesized materials were determined by nitrogen physisorption using a Micromeritics TriStar instrument. Inorganic samples were degassed at 150 °C and at a pressure below 100 mTorr for a minimum of 4 h and hybrid membranes at 80 °C for 16 h prior to analysis using a Micromeritics VacPrep 061. Surface areas were calculated using the Brunauer−Emmett−Teller (BET) method. The Barrett−Joyner−Halenda (BJH) method was used to calculate the pore size distribution. To estimate the pore volume of pores ≤8 nm in diameter, the total pore volume at the single point $p/p_0 = 0.736$ on the adsorption curve was used, corresponding to the volume of mesopores ≤8 nm in diameter. The pore volume of pores >8 nm in diameter was equivalent to the total pore volume minus the volume of pores ≤8 nm in diameter.

Scanning electron microscopy (SEM) was performed on a FEI QUANTA 200F microscope operated at voltages between 15 and 20 kV. Samples were mounted on carbon-coated SEM stubs and then sputter-coated with a thin layer of gold using an Edwards S150B gold sputter coater.

The crystallinity of the prepared materials was analyzed using X-ray diffraction (XRD). The finely ground samples were analyzed from 10 to 80° 2θ on a Siemens D500 diffractometer equipped with a curved graphite crystal monochromator and a Scintag X1 diffractometer fitted with a Peltier detector. Copper Kα radiation at 40 kV and 30 mA was used with a step size of 0.02° 2θ and an integration time of 1 s per step. Data sets were analyzed using XPLOT for Windows (version 1.34) and the International Center for Diffraction Data Database (sets 1−54).

Nonambient XRD patterns were recorded on a PANalytical X'Pert Pro diffractometer using copper Kα radiation and an X'Celerator detector employing real-time multiple strip detection. Heating of the sample was achieved using a programmable Anton-Parr HTK-2000 furnace accessory.

Transmission electron microscopy (TEM) was conducted using a JEOL FX2000 microscope operating at 200 keV. TEM samples were prepared by finely grinding the sample in ethanol followed by sonicating for 20 min before drop-depositing the material on to carbon-coated copper grids.

Dynamic light scattering (DLS) experiments were performed on 1 mg mL^{-1} PEI solutions at pH 10 using a Malvern Instruments Nano-ZS Zetasizer at 25 °C. The solutions were filtered through Millipore nylon filters (pore size 0.45 μm). The normalized intensity autocorrelation function $g_2(t)$ was measured and analyzed according to the CONTIN method using Dispersion Technology Software v5.03 (Malvern Instruments). This analysis resulted in a discrete, intensity-weighted distribution function of logarithmically equidistant-spaced decay time. The hydrodynamic diameters were calculated from the corresponding

decay times using the Stokes−Einstein equation. The hydrodynamic diameters of the polymers were found to be 1.2 ± 0.2, 2.0 ± 0.1, and 11.0 ± 1.8 nm for the respective molecular weights of 1300, 25 000, and 600 000−1 000 000 Da.

Templating. A 15 wt % precursor solution was prepared by combining 97% titanium(IV) isopropoxide (100 g, 0.34 mol) with 70% zirconium(IV) propoxide (70 g, 0.15 mol) and 2-propanol (830 g) to produce a Zr to Ti ratio of 30:70 mol %. The membranes were placed in a container, covered with the precursor solution, and stirred for 5 min. Using tweezers, the membranes were then transferred to a solution of 1:1 water−2-propanol, by volume, and stirred for an additional 5 min. The coated membranes were removed from solution, slightly dried on a paper towel, and then pressed between glass slides. Stacks of glass slides were held together using binder clips. The membranes were dried at 60 °C for a minimum of 6 h. Multiple coats were applied until the membranes were ∼150% of the original mass, which ranged from three to seven coatings, depending on the surface area of the template. All five templated materials were calcined under air at 550 °C for 5 h with a ramp rate of 2.9 °C min^{-1} from room temperature. The nomenclature is as follows. Organic membranes are referred to by their abbreviation: for example, GHP 0.45 μm is a GH Polypro membrane with a particle retention of 0.45 μm. The templated and calcined metal oxide membrane is labeled ZrTi-membrane: for example, ZrTi-GHP 0.45 μm.

Incorporation of PEI into Metal Oxide Membranes. Metal oxide membranes were impregnated with three molecular weights of polymer. The general procedure (15) was as follows: PEI was dissolved in Milli-Q water, and the volume was adjusted to produce a 9 wt % PEI solution. Prior to pH adjustment, the solution containing dissolved PEI had a pH of approximately 11.8, which was altered to pH 10 using 1 M HCl. The metal oxide support (0.05 g) was added to 1.5 g of PEI solution and gently swirled for 24 h before draining and applying three 1 h long soaks in pH 10 water (pH adjusted with 0.01 M KOH) to remove any of the unbound PEI from the metal oxide support. The pH of the dissolved 25 000 Da PEI solution was adjusted to pH 8, 9, 10, and 10.6 using 0.1 M HCl, for the study of pH effect pertaining to Figure 6. Portions of ZrTi-GHP 0.2 μm (0.05 g) were exposed to these sorption solutions (1.5 g). The membranes were stirred for 24 h before draining and soaking in an aqueous solution of the corresponding pH three times over the course of 4 h.

Polymer loading was estimated using eq 1.

$$\text{loading (mg g}^{-1}) = (M_H - M_{MO}) \times 10 \qquad (1)$$

where M_H is the percent weight loss of the hybrid material determined by TGA, M_{MO} is the percent weight loss of the metal oxide membrane solely, and the factor 10 is to convert from a percentage into milligrams of weight lost per gram of material. For example, if the total weight loss was 8% (M_H) and the metal oxide had a weight loss of 2% (M_{MO}), the loading would be 60 mg g^{-1}. To normalize for surface area, the loading (mg g^{-1}) was divided by the surface area (m^2 g^{-1}) of the metal oxide membrane, and to normalize for pore volume, the loading (mg g^{-1}) was divided by the pore volume (cm^3 g^{-1}) of the material.

RESULTS AND DISCUSSION

Characterization of the Organic Membranes. Pore size control is important in a support. The fundamental study by Dubin and co-workers (14) found that mesoporous supports containing 8 nm pores require 48 h to reach equilibrium; however, materials with pores 285 nm in diameter reach equilibrium in essentially the same time frame as nonporous materials. Therefore, a hierarchical pore structure may allow the interior mesoporous network to be rapidly accessed by solution. Such a complex structure is easily achievable using templates.

Templating allows the pore structure of an organic material to be imparted to an inorganic material. Membrane templates were chosen for this work because they have previously been shown to have defined macropore and mesopore sizes. For the formation of zirconium titanium oxide membranes (denoted ZrTi-x, where x indicates the template used) with a Zr to Ti mole ratio of 3:7, five commercially available membranes were studied as templates: cellulose acetate (CA), GH Polypro 0.2 μm (GHP 0.2 μm), GH Polypro 0.45 μm (GHP 0.45 μm), Nylaflo (NY), and Versapore (VERS). GHP 0.2 μm and GHP 0.45 μm were very similar in most respects, and so characterization will focus on GHP 0.2 μm and only the physical properties of GHP 0.45 μm required for a comparison of PEI adsorption are reported. Mixed metal oxides have some benefits over single oxides, including increased surface acidity, thermal stability, mechanical strength, and surface area (38). The mixed oxide membranes displayed a higher surface area compared to the single oxide titania (surface area 74 m^2 g^{-1}) or zirconia (surface area 54 m^2 g^{-1}) membranes templated from CA and calcined at 400 °C (20). A Zr content of 30−40 mol % within a titania matrix has proven to yield the highest surface area, although the exact percentage is dependent on processing conditions (39).

To ensure an even coating and a faithful reproduction of the template morphology, the organic membranes were repeatedly coated with a 15 wt % solution of alkoxide in 2-propanol (22). It is evident from SEM images in Figure 1 that there were similarities between the structure of the templates and the calcined inorganic membranes (see Figure S1 in the Supporting Information for lower magnification cross-sectional views of the membrane). The size of the macropores in the templated inorganic membranes is shown in TEM images of the ultramicrotomed sample (Figure 1c,f,i,l).

The mesopore structure can be seen in TEM images of the metal oxide materials in Figure 2. Notably, the templates CA, NY, and VERS produced metal oxides with mesostructures very different from that of GHP 0.2 μm. The metal oxides templated from CA, VERS, and (to a lesser degree) NY show the presence of regularly shaped and evenly spaced particles. The template GHP 0.2 μm produced a metal oxide with less well-defined nanoparticles; hence, this sample lacked the small interparticle mesopores present in the other three materials.

A variety of pore sizes, surface areas, and pore volumes were obtained in the metal oxide membranes (Table 1 and Figure 3; see Figure S2 in the Supporting Information for sorption isotherms). The nitrogen sorption data showed two distinct mesopore size distributions: a small mesopore (≤8 nm in diameter) and a larger mesopore (≥11 nm in diameter) extending through the macropore region (≥50 nm in diameter). The macropores and large mesopores resulted

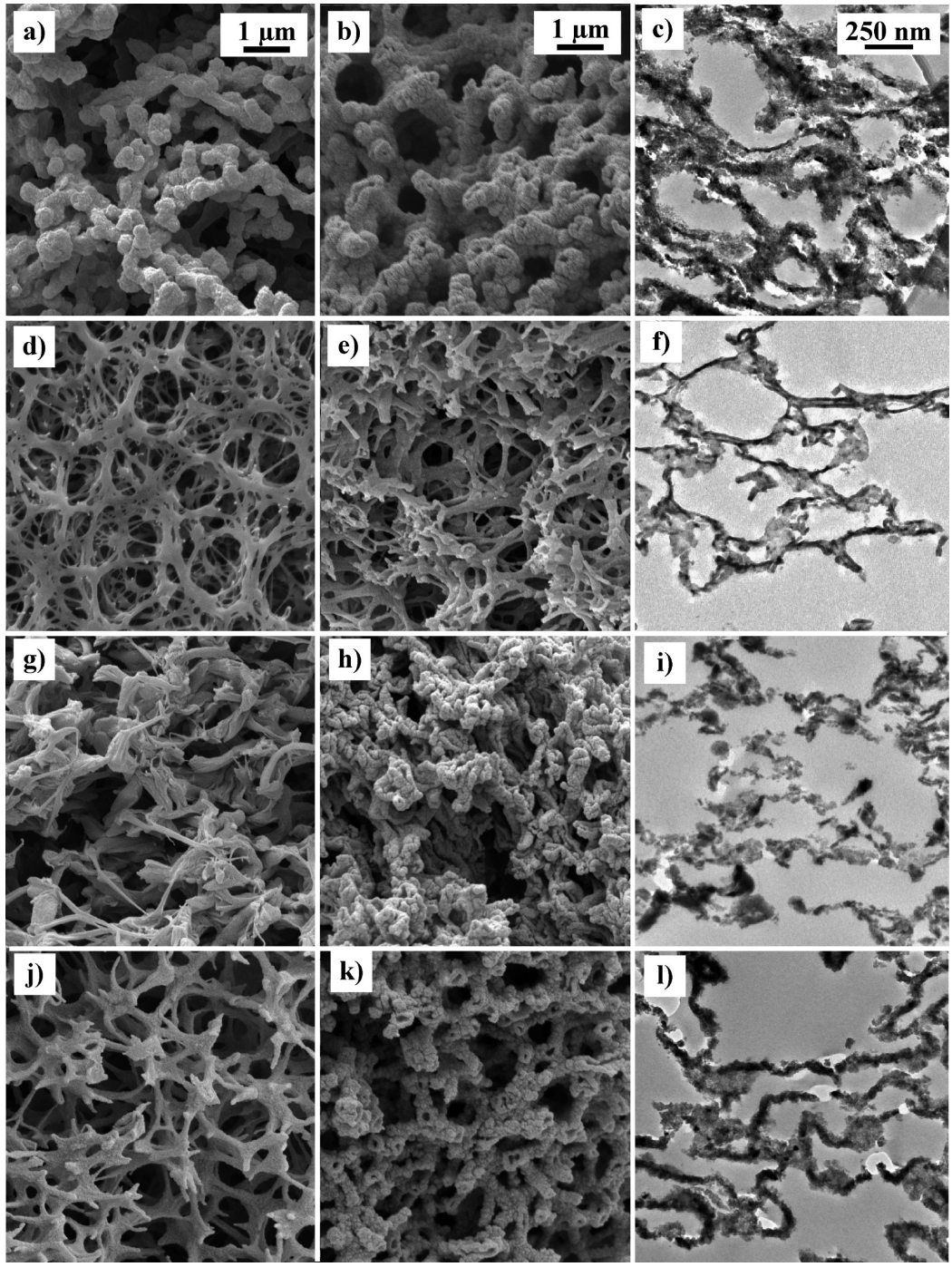

FIGURE 1. Cross-sectional SEM images of the template membranes: (a) CA; (d) GHP 0.2 μm; (g) NY; (j) VERS. Cross -sectional SEM images of the resulting metal oxides: (b) ZrTi-CA; (e) ZrTi-GHP 0.2 μm; (h) ZrTi-NY; (k) ZrTi-VERS. TEM images of ultramicrotomed samples: (c) ZrTi-CA; (f) ZrTi-GHP 0.2 μm; (i) ZrTi-NY; (l) ZrTi-VERS. The scale bar at the top of each column is the same scale for all samples shown below.

from templating the membrane structure, whereas the small mesopores were due to interparticulate voids. The GHP 0.2 and 0.45 μm templates produced substantially different mesoporosities compared with the other templates (see Figure S3 in the Supporting Information for a comparison of the pore size distributions of ZrTi-GHP 0.2 and 0.45 μm). It is possible that this difference in architecture is due to differences in combustion of the templates during calcination. For instance, ZrTi-CA, ZrTi-NY, and ZrTi-VERS had at least double the surface area of ZrTi-GHP 0.2 and 0.45 μm. This higher surface area was likely due to the presence of pores in the small mesopore range; for both ZrTi-GHP 0.2 and 0.45 μm membranes the pore volume was very small for pores of less than 11 nm diameter. The absence of small mesopores exhibited by ZrTi-GHP 0.2 and 0.45 μm indicates that there were no well-defined nanoparticles, which is consistent with what can be observed in the TEM image (Figure 2).

The homogeneity of the zirconium and titanium in the inorganic membrane structures was determined by monitoring the crystallization of the oxide with nonambient XRD (Figure 4). The samples did not undergo a phase change

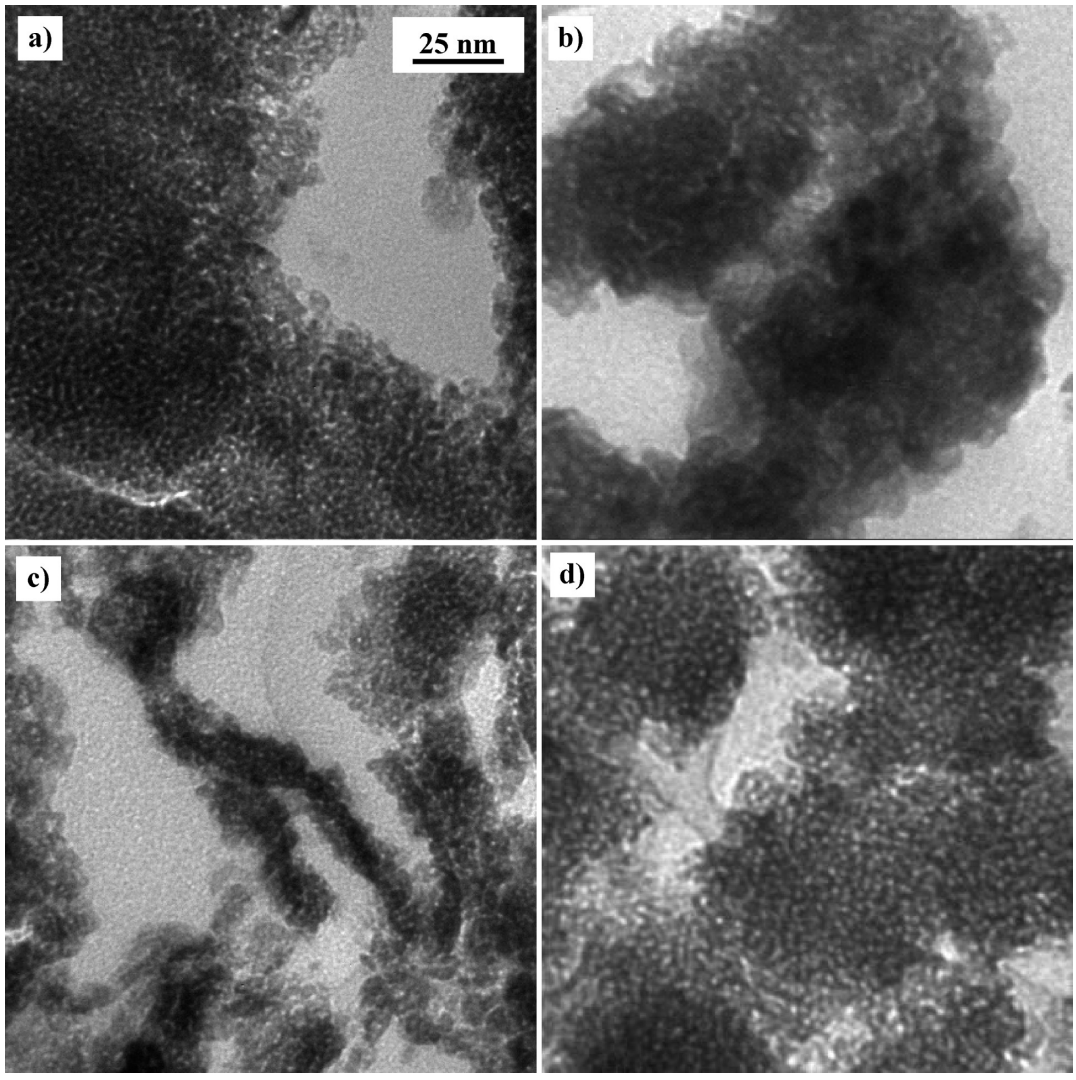

FIGURE 2. TEM images: (a) ZrTi-CA; (b) ZrTi-GHP 0.2 μm; (c) ZrTi-NY; (d) ZrTi-VERS. Samples were prepared by grinding and drop -depositing on TEM grids. The scale bar is the same for all images.

Table 1. Surface Area and Pore Volume of the Zirconium Titanium Oxides Templated from GHP 0.2 and 0.45 μm and 0.2 μm CA, NY, and VERS Obtained from Nitrogen Sorption Data

		pore volume ($cm^3\ g^{-1}$)	
membrane	surface area ($m^2\ g^{-1}$)	pore diam ≤8 nm[a]	pore diam >8 nm[b]
ZrTi-GHP 0.2 μm	47 ± 11	0.04 ± 0.003	0.18 ± 0.02
ZrTi-GHP 0.45 μm	57 ± 10	0.05 ± 0.001	0.12 ± 0.03
ZrTi-CA	91 ± 11	0.07 ± 0.003	0.07 ± 0.01
ZrTi-NY	125 ± 13	0.09 ± 0.002	0.16 ± 0.02
ZrTi-VERS	131 ± 15	0.11 ± 0.006	0.10 ± 0.01

[a] The total pore volume at the single point $p/p_0 = 0.736$ on the adsorption curve, corresponding to the volume of pores ≤8 nm in diameter and less. [b] Total pore volume at the single point $p/p_0 = 0.988$ on the adsorption curve minus the volume of the small mesopore (≤8 nm) volume.

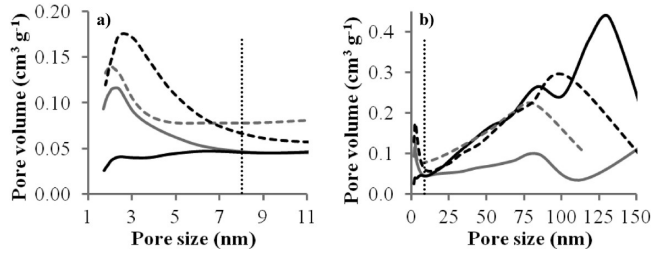

FIGURE 3. Pore size distribution determined from gas sorption data highlighting the (a) small mesopore size and (b) large mesopore to macropore size distribution of ZrTi-GHP 0.2 μm (solid black line), ZrTi-CA (solid gray line), ZrTi-NY (dotted gray line), and ZrTi-VERS (dotted black line). The dotted line at 8 nm marks the lower limit of the large mesopore.

from amorphous to any of the pure crystal forms of titania (i.e., anatase, brookite, or rutile) or zirconia with heating; however, a hint of the srilankite phase becomes evident. The presence of the srilankite crystal phase ($Zr_{0.3}Ti_{0.7}O_2$), the high onset of crystallization, and the lack of either pure metal oxide crystals at these high temperatures suggests that zirconium and titanium were homogeneously dispersed in the mixed oxide. The hint of crystallinity was first evident by XRD analysis at 500 °C for ZrTi-CA and ZrTi-VERS and at 400 °C for ZrTi-GHP 0.2 μm and ZrTi-NY. Srilankite crystallization was less obvious in the XRD patterns of the materials calcined (550 °C, 5 h) in bulk (see Figure S4 in the Supporting Information). As stated before, many physical

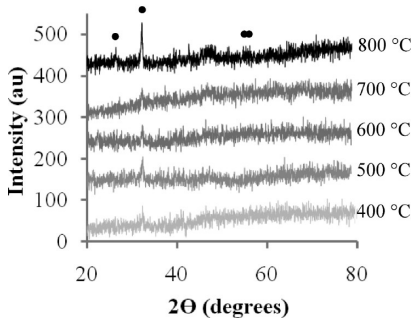

FIGURE 4. XRD plot of ZrTi-GHP 0.2 μm heated from 400−800 °C, showing that the material turns from amorphous to partially crystalline srilankite. The positions of srilankite peaks are indicated by dots. Each sequential temperature plot is shifted upward by 100 au.

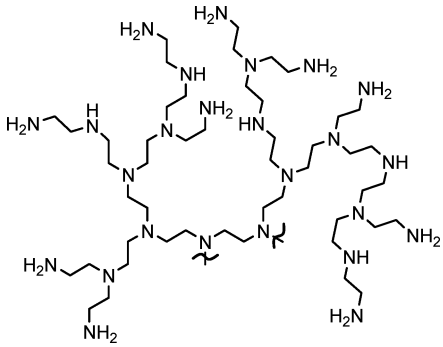

FIGURE 5. Example of the molecular structure of a hyperbranched polyethyleneimine polymer, showing the presence of primary, secondary, and tertiary amine functionalities.

properties are enhanced by mixing two oxides; thus, the production of molecularly mixed zirconium titanium oxides is a benefit of this templating technique.

Incorporation of PEI into the Porous Inorganic Supports. PEI interacts with the metal oxides through hydrogen bonding and electrostatic interactions (36), with the strength of the attractive force being dependent upon the pH. The shape and size of PEI have been reported to remain fairly constant between pH 2 and 10, as this polyelectrolyte is branched and thus globular in shape (28). Therefore, any changes in the degree of incorporation will be primarily due to the strength of the electrostatic interaction between the polymer and the oxide surface. The structure of PEI is shown in Figure 5. Hydrogen bonding occurs through the surface O−H groups on the metal oxide and the N−H groups of the polymer. An electrostatic attraction can occur between positively charged PEI and negatively charged metal oxide surfaces, whereas electrostatic repulsion occurs when the polymer and oxide have the same charge. Furthermore, the surface of a titania-rich mixed oxide contains Lewis acid sites due to coordinative unsaturation of metal centers (39, 40), and amines are Lewis bases; hence, an acid−base interaction can occur in addition to electrostatic attraction.

The solution pH during incorporation determines the quantity of the polymer incorporated onto the metal oxide surface. In order to investigate the influence of pH, ZrTi-GHP 0.2 μm was placed in 9 wt % solutions of 25 000 Da PEI ranging in pH from 8 to 10.6, and the mixture was agitated

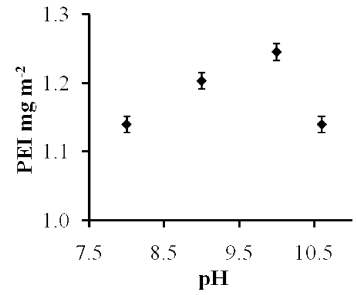

FIGURE 6. Adsorption of 25 000 Da PEI as a function of pH onto ZrTi-GHP 0.2 μm.

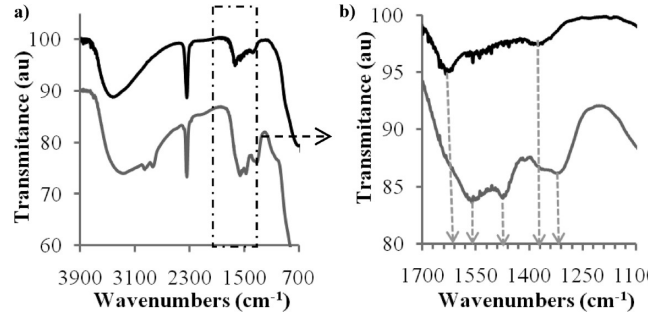

FIGURE 7. (a) ATR FTIR transmission spectrum of ZrTi-GHP 0.2 μm (black line) and ZrTi-GHP 0.2 μm impregnated with 600 000 Da PEI (gray line) and (b) an expansion between the wavenumbers of 1700 and 1100 cm^{-1}.

for 24 h. ZrTi-GHP 0.2 μm was chosen to study the electrostatic interaction between the polymer and the metal oxide because it had the highest PEI loading capacity (discussed later). It was assumed that the other metal oxides had optimal polyelectrolyte adsorption at the same pH, since their surfaces should have similar charge density and electrokinetic potential. Zirconium titanium oxides of the molar composition studied here are negatively charged at pH higher than ~5.5 (39). However, the amino groups along the PEI backbone range from largely positively charged below pH 8 to mostly neutral at pH 11 (27). Of the pH values studied, the maximum adsorption of PEI occurred at pH 10 (Figure 6); thus, all further experiments were carried out at pH 10. The optimal pH for 10 000 Da PEI loading onto titania nanoparticles was found to be pH 10.2 (34), similar to the results acquired here.

To ensure that the PEI was attaching to the metal oxide surface, ATR-FTIR spectra were acquired of ZrTi-GHP 0.2 μm and ZrTi-GHP 0.2 μm incorporated with PEI bearing octyl chains (Figure 7). It is known that the decoration of zirconia with amines gives rise to two absorption bands (bending modes) in the wavenumber ranges 1560−1580 and 1350−1450 cm^{-1} (34). The ATR-FTIR spectrum of PEI-impregnated ZrTi-GHP 0.2 μm exhibited three new bands at 1562, 1475, and 1315 cm^{-1}. The last of these three bands does not correspond to the free amine (34) and thus can probably be attributed to a titanium−amine interaction. The appearance of the PEI−zirconium bending modes is consistent with the Lewis acid−base interaction of PEI with the metal oxide surface.

To study whether PEI was filling the mesopores or solely adsorbing onto the external and macropore surfaces, gas

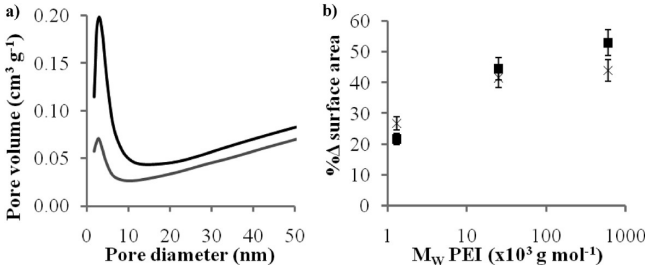

FIGURE 8. (a) BJH pore size distribution of ZrTi-VERS (black line) and ZrTi-VERS impregnated with 600 000−1 000 000 M_w PEI (gray line). The impregnated ZrTi-VERS material was normalized for the weight of the metal oxide. (b) The percentage decrease in the surface area of impregnated ZrTi-GHP 0.2 μm (■) and ZrTi-VERS (×) as a function of PEI molecular weight. ZrTi-CA and ZrTi-NY decorated with 600 000−1 000 000 M_w PEI displayed decreases in surface area of 41% and 44%, respectively.

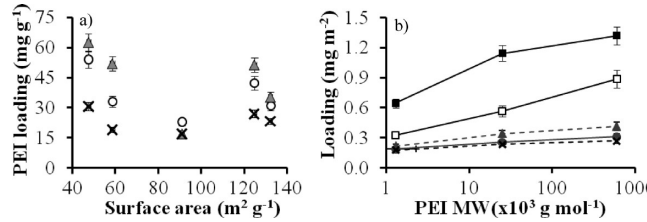

FIGURE 9. (a) Adsorption of 1300 Da (×), 25 000 Da (○), and 600 000−1 000 000 Da (▲) PEI at pH 10 as a function of surface area. There is no correlation between the quantity of PEI adsorbed and the surface area of the metal oxide support (R^2 values ranged from 0.01 to 0.19). (b) Adsorption of PEI of different molecular weights at pH 10, normalized for surface area. The samples are depicted as follows: (■) ZrTi-GHP 0.2 μm; (□) ZrTi-GHP 0.45 μm; (●) ZrTi-CA; (◆) ZrTi-NY; (×) ZrTi-VERS. Error bars denote standard deviation, and where they cannot be seen, the error is less than the size of the marker.

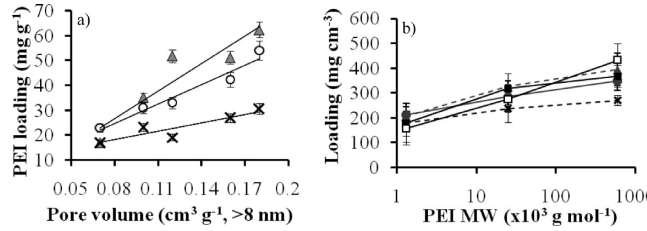

FIGURE 10. (a) Adsorption of 1300 Da (×), 25 000 Da (○), and 600 000 Da (▲) PEI at pH 10 as a function of the pore volume of pores >8 nm in diameter. The R^2 factor ranged from 0.82 to 0.95, showing that as pore volume increases, so does the capacity for PEI adsorption. (b) Adsorption of PEI of different molecular weights at pH 10, normalized for the pore volume of pores >8 nm in diameter. The samples are depicted as follows: (■) ZrTi-GHP 0.2 μm; (□) ZrTi-GHP 0.45 μm; (●) ZrTi-CA; (▲) ZrTi-NY; (×) ZrTi-VERS. Error bars denote standard deviation, and where they cannot be seen, the error is less than the size of the marker.

sorption experiments were performed on the decorated materials. It was reported that the pore size of macroporous alumina membranes shrank upon incorporation of the alumina membranes with PEI of 5000 Da (25). ZrTi-VERS decorated with 600 000−1 000 000 Da PEI was chosen as an example (Figure 8a) because ZrTi-VERS had the highest mesopore volume. The largest molecular weight of PEI was used because it is the most likely to be excluded from the smallest diameter pores. The pore size distribution over the mesoporous range indicated that some of the smallest mesopores were filled or blocked, rendering some pore volume inaccessible. However, some portion of the mesopores was still detected, indicating that not all of the pore volume was obstructed by the polymer. The surface area of impregnated ZrTi-VERS and ZrTi-GHP 0.2 μm decreased (Figure 8b), as well as the pore volume, indicating once again that the entrances to pores were blocked, or the pores filled, by PEI. The stabilization in surface area between ZrTi-VERS incorporated with 25 000 and 600 000−1 000 000 Da PEI correlates well with the lack of increased PEI loading of ZrTi-VERS between those molecular weights.

Incorporation of large macromolecules (2−11 nm in hydrodynamic diameter) into porous silica nanoparticles has been shown to be highly dependent on the size of the mesopore (14, 15). Thus, for the present study, the diameter of the three molecular weights of dissolved PEI was measured at pH 10 using DLS. The hydrodynamic diameters of the polymers were 1.2 ± 0.2, 2.0 ± 0.1, and 11.0 ± 1.8 nm for the respective molecular weights of 1300, 25 000, and 600 000−1 000 000 Da. To investigate the relationship between the properties of the inorganic membrane and uptake of PEI, the five metal oxide membranes were impregnated with PEI bearing octyl chains of differing molecular weights (Figures 9 and 10). Loading increased with increasing molecular weight, particularly for ZrTi-GHP 0.2 and 0.45 μm, which had mostly large pores (>11 nm). It should be noted that maximum loading in these macroscopic inorganic membranes is 1.25 mg m^{-2}, which is higher than the 0.80 mg m^{-2} achieved by the mesoporous silica nanoparticles reported by Wang and co-workers (15).

In macroporous systems, polymer loading has been reported to be proportional to the surface area of the solid support (25); however, in this hierarchically porous system no relationship was evident, regardless of polymer molecular weight (Figure 9a). Intuitively, a larger surface area should provide a greater degree of incorporation because there is more surface to which the polymer may attach. However, the opposite trend was observed: as surface area increased, polymer loading decreased. To explore this surprising correlation between surface area and polymer loading, the results were plotted as a function of PEI adsorbed per square meter of surface (Figure 9b). It was clear that the surfaces in each inorganic membrane were not equally accessible. Impregnated ZrTi-GHP 0.2 μm displayed the highest quantity of PEI, followed by ZrTi-GHP 0.45 μm. The most obvious difference between the GHP templates and the other templates is the lack of a small interparticle mesopore (≤8 nm). Small mesopores add a great deal of surface area, but large molecules will not necessarily be able to enter the confined space of these small mesopores. The exclusion of the smallest molecular weight polymer from the three oxide membranes with small mesopore diameters was due to the viscosity of the solution and inter-/intramolecular PEI interactions, rather than a size mismatching between the relatively small polymer and the mesopore diameter. High surface areas are of little utility if the pores inhibit macromolecular entry.

The total pore volume also showed very poor correlations with polymer adsorption ($R^2 = 0.18-0.52$; Figure S5 in the

Supporting Information). The amount of polyelectrolyte adsorbed should be dependent on the pore volume, because often polyelectrolytes do not often lie flat on the surface of a support, but rather coil and loop into free space (14). The polymer used in this study has a roughly spherical shape due to the fact that it is hyperbranched and thus will extend from the surface. PEI loading, as a function of the pore volume, gave plots that were reasonably linear when the contribution from small mesopores (≤8 nm, see footnote to Table 1) was eliminated (Figure 10a). The emergence of a trend only after this correction to the pore volume once again suggests that polymer access to the pores of small diameter is limited. This phenomenon may be related to the viscosity of the solution, but the end result is the same.

The pore volume effect can be further accentuated by comparing PEI loading between ZrTi-GHP 0.2 and 0.45 μm, which had similar pore size distributions (see Figure S3 in the Supporting Information) but differing pore volumes (Table 1). With the pore diameter normalized, it was clear that pore volume and pore loading increased proportionally. For instance, ZrTi-GHP 0.45 μm had 67% as much large pore volume (pores >8 nm) and adsorbed 70% as much 600 000–1 000 000 Da PEI as ZrTi-GHP 0.2 μm. All of the inorganic supports performed similarly when the adsorption results were normalized for the pore volume of the large pores (Figure 10b), signifying that the surface of large mesopores and macropores was equally accessible between the materials.

The main conclusion from this data is that the majority of the incorporation occurred on the surface of the macropores and large mesopores when polymer solutions of 9 wt % and of pH 10 were used. Therefore, pore size and pore volume are much more important factors than surface area for polymer loading properties within mesoporous materials. Thus, when inorganic supports are designed for this purpose, a template which forms a large mesopore is most desirable. These findings are applicable to many materials, including drug delivery vehicles (15), enzyme-impregnated chromatography columns (41), and optical materials that have been postsynthetically modified with photochromic polymers (42).

CONCLUSIONS

Five organic membranes were used as templates to produce zirconium titanium oxide membranes. The macropore architecture of the template was successfully replicated by the inorganic material. The templating technique also gave rise to differing mesopore architectures. Thus, through sol–gel and template synthesis, homogeneously mixed zirconium titanium oxide materials with well-defined and distinct pore size distributions, pore volumes, and surface areas were produced.

These inorganic membranes were impregnated with PEI bearing octyl chains from 9 wt % solutions at pH 10. High adsorption capacities were attained (1.25 mg m^{-2}). The surface area, pore size, and pore volume of these hierarchically porous materials were studied with regard to how these properties influence attachment of PEI onto metal oxide surfaces. The inorganic membrane ZrTi-GHP 0.2 μm displayed the highest loading capacity for PEI, a fact which is attributed to the structure of the inorganic membrane. The majority of the pore volume in this material consisted of pores >11 nm in diameter, which meant that the majority of the surface was accessible to the large polymers. It was found that even the smallest molecular weight PEI (with a hydrodynamic diameter of 1.2 nm) showed a greater degree of incorporation into GHP-templated membranes. Although this finding is attributable to the viscosity and inter-/intramolecular interactions of the PEI in solution, the end result is that a material with large mesopores yields higher polymer loading. The mesopore size of the solid supports seemed to be the most important factor influencing polymer loading, followed by the quantity of pore volume of pores >8 nm in diameter. Surface area was not an important factor, because much of the internal mesopore surface was inaccessible to macromolecules in those materials possessing small mesopores. This finding indicates that mesopore diameter and volume should be considered when designing porous materials to adsorb macromolecules: high surface areas are obtainable by preparing structures with small mesopores, but the bulk of this surface area will be inaccessible to large molecules.

Acknowledgment. Massey de los Reyes and Paolo Imperia are thanked for conducting nonambient X-ray diffraction experiments. Infrared spectroscopy was performed in the laboratory of Dr. Galo J. de A. A. Soler-Illia with the help of Alejandra Calvo. This work was financially supported by a Discovery Project from the Australian Research Council (No. DP0877428), Awards (Nos. AINGR07025 and AINGR08012) from the Australian Institute of Nuclear Science and Engineering, and an ANSTO/University of Melbourne Collaborative Research Support Scheme.

Supporting Information Available: Figures giving SEM images of the membrane cross-section and the templated inorganic membranes, nitrogen sorption isotherms, pore size distributions of ZrTi-GHP 0.2 μm and ZrTi-GHP 0.45 μm, XRD patterns of calcined inorganic membranes, and the PEI loading as a function of total pore volume and a table detailing polymer loading. This material is available free of charge via the Internet at http://pubs.acs.org.

REFERENCES AND NOTES

(1) Okada, A.; Usuki, A. *Soc. Automot. Eng., [Spec. Publ.] SP* **2007**, *SP-2113*, 49.
(2) Somasundaran, P.; Mehta, S. C.; Rhein, L.; Chakraborty, S. *MRS Bull.* **2007**, *32*, 779.
(3) Jeong, S.; Kim, D.; Moon, J. *J. Phys. Chem. C* **2008**, *112*, 5245.
(4) Gautier-Luneau, I.; Denoyelle, A.; Sanchez, J. Y.; Poinsignon, C. *Electrochim. Acta* **1992**, *37*, 1615.
(5) Burnside, S. D.; Brooks, K.; McEvoy, A. J.; Michael, G. *Chimia* **1998**, *52*, 557.
(6) Avnir, D.; Coradin, T.; Lev, O.; Livage, J. *J. Mater. Chem.* **2006**, *16*, 1013.
(7) Calvo, A.; Yameen, B.; Williams, F. J.; Azzaroni, O.; Soler-Illia, G. J. de A. A *Chem. Commun.* **2009**, *18*, 2553.
(8) Sanchez, C.; Julián, B.; Belleville, P.; Popall, M. *J. Mater. Chem.* **2005**, *15*, 3559.
(9) Fryxell, G. E. *Inorg. Chem. Commun.* **2006**, *9*, 1141.
(10) Müller, U.; Schubert, M. M.; Yaghi, O. M. Chemistry and Applications of Porous Metal-Organic Frameworks. In *Handbook of Heterogeneous Catalysis*, 2nd ed.; Ertl, G., Knözinger, H., Schüth, F., Weitkamp, J., Eds.; Wiley-VCH: Weinheim, Germany, 2008.

(11) Wang, Y.; Caruso, F. *Chem. Mater.* **2006**, *18*, 4089.
(12) Huang, J.; Ichinose, I.; Kunitake, T. *Angew. Chem., Int. Ed.* **2006**, *45*, 2883.
(13) Cunin, F.; Li, Y. Y.; Sailor, M. J. *BioMEMS Biomed. Nanotech.* **2006**, *3*, 213.
(14) Mishael, Y. G.; Dubin, P. L.; de Vries, R.; Kayitmazer, A. B. *Langmuir* **2007**, *23*, 2510.
(15) Wang, Y.; Angelatos, A. S.; Dunstan, D. E.; Caruso, F. *Macromolecules* **2007**, *40*, 7594.
(16) Otal, E. H.; Angelomé, P. C.; Aladabe-Bilmes, S.; Soler-Illia, G. J. d. A. A. *Adv. Mater.* **2006**, *18*, 934.
(17) Angelomé, P. C.; Soler-Illia, G. J. d. A. A. *Chem. Mater.* **2005**, *17*, 322.
(18) Angelomé, P. C.; Aldabe-Bilmes, S.; Calvo, M. E.; Crepaldi, E. L.; Grosso, D.; Sanchez, C.; Soler-Illia, G. J. d. A. A. *New J. Chem.* **2005**, *29*, 59.
(19) Jing, W.; Huang, W.; Xing, W.; Wang, Y.; Jin, W.; Fan, Y. *ACS Appl. Mater. Interfaces* **2009**, *1*, 1607.
(20) Caruso, R. A.; Schattka, J. H. *Adv. Mater.* **2000**, *12*, 1921.
(21) Caruso, R. A.; Antonietti, M. *Adv. Funct. Mater.* **2002**, *12*, 307.
(22) Schattka, J. H.; Wong, E. H.-M.; Antonietti, M.; Caruso, R. A. *J. Mater. Chem.* **2006**, *16*, 1414.
(23) Shchukin, D. G.; Caruso, R. A. *Adv. Funct. Mater.* **2003**, *13*, 789.
(24) Tang, F.; Uchikoshi, T.; Ozawa, K.; Sakka, Y. *J. Eur. Ceram. Soc.* **2006**, *26*, 1555.
(25) Tsetsekou, A.; Arkas, M.; Kritikaki, A.; Simonetis, S.; Tsiourvas, D. *J. Membr. Sci.* **2008**, *311*, 128.
(26) Arkas, M.; Allabashi, R.; Tsiourvas, D.; Mattausch, E.-M.; Perfler, R. *Environ. Sci. Technol.* **2006**, *40*, 2771.
(27) Ghoul, M.; Bacquet, M.; Morcellet, M. *Water Res.* **2003**, *37*, 729.
(28) Kobayashi, S.; Hiroishi, K.; Tokunoh, M.; Saegusa, T. *Macromolecules* **1987**, *20*, 1496.
(29) Nonogaki, S.; Makishima, S.; Yoneda, Y. *J. Appl. Polym. Sci.* **1958**, *41*, 195.
(30) Nishide, H.; Deguchi, J.; Tsuchida, E. *Chem. Lett.* **1976**, *0*, 169.
(31) Navarro, R. R.; Sumi, K.; Matsumura, M. *Water Res.* **1999**, *33*, 2037.
(32) Amara, M.; Kerdjoudj, H. *Desalination* **2004**, *168*, 195.
(33) Juttukonda, V.; Paddock, R. L.; Raymond, J. E.; Denomme, D.; Richardson, A. E.; Slusher, L. E.; Fahlman, B. D. *J. Am. Chem. Soc.* **2006**, *128*, 420.
(34) Chaufer, B.; Rabiller-Baundry, M.; Bouguen, A.; Labbé, J. P.; Quémerais, A. *Langmuir* **2000**, *16*, 1852.
(35) McNeff, C.; Zhao, Q.; Almlof, E.; Flickinger, M.; Carr, P. W. *Anal. Biochem.* **1999**, *274*, 181.
(36) Wang, J.; Gao, L. *Nanostruct. Mater.* **1999**, *11*, 451.
(37) McNeff, C.; Carr, P. W. *Anal. Chem.* **1995**, *67*, 3886.
(38) Reddy, B. M.; Khan, A. *Catal. Rev.* **2005**, 257.
(39) Drisko, G. L.; Luca, V.; Sizgek, E.; Scales, N.; Caruso, R. A. *Langmuir* **2009**, *25*, 5286.
(40) Tanabe, K.; Takashi, S.; Shibata, K.; Kiyoura, T.; Kitagawa, J. *Bull. Chem. Soc. Jpn.* **1974**, *47*, 1064.
(41) Reshmi, R.; Sanjay, G.; Sugunan, S. *Catal. Commun.* **2007**, *8*, 393.
(42) Sanchez, C.; Ribot, F.; Lebeau, B. *J. Mater. Chem.* **1999**, *9*, 35.

AM9006098